Research article

Radoslaw Kolkowski and A. Femius Koenderink*

Gain-induced scattering anomalies of diffractive metasurfaces

https://doi.org/10.1515/nanoph-2020-0253
Received April 24, 2020; accepted July 5, 2020; published online July 26, 2020

Abstract: Photonic nanostructures with gain and loss have long been of interest in the context of diverse scattering anomalies and light-shaping phenomena. Here, we investigate the scattering coefficients of simple gain-doped diffractive metasurfaces, revealing pairs of scattering anomalies surrounded by phase vortices in frequency–momentum space. These result from an interplay between resonant gain, radiative loss, and interference effects in the vicinity of Rayleigh anomalies. We find similar vortices and singular points of giant amplification in angle-resolved reflectivity spectra of prism-coupled gain slabs. Our findings could be of interest for gain-induced wavefront shaping by all-dielectric metasurfaces, possibly employing gain coefficients as low as ~50 cm^{-1}.

Keywords: active nanophotonics; dielectric nanoparticles; metasurfaces; nanoparticle arrays; phase singularities.

1 Introduction

Electromagnetic metasurfaces are two-dimensional (2D) arrays of scatterers used to control amplitude, phase, and polarization of reflected, transmitted, and diffracted electromagnetic waves [1–4]. Recently, extensive research has been devoted to combining metasurfaces with gain media, with the main focus on distributed feedback lasing and diffractive outcoupling in plasmonic and dielectric nanoparticle arrays [5]. These studies largely relate to the notion of combining gain with surface lattice resonances [6], in which Rayleigh anomalies and plasmon particle resonances hybridize [7]. Recent theoretical works suggest that, apart from lasing, the role of gain could be far more nontrivial. For instance, properly engineered gain and loss could overcome efficiency barriers of metasurfaces for wavefront transformation imposed by impedance mismatch [8, 9], mitigate constraints on electric and magnetic optical response of matter [10, 11], and control the scattering by small ensembles of nano-objects [12, 13]. The interplay between gain and loss gives rise to many scattering anomalies [14], such as unidirectional invisibility, coherent perfect absorber-lasers, as well as manifestations of parity–time (PT) symmetry [15–17], offering a platform for active control of light propagation [18–20] and for enhanced light-matter interactions [21–23].

In this work, we theoretically demonstrate the existence of scattering anomalies embedded in the band structure of simple diffractive arrays of identical dielectric nanoparticles (Figure 1, left) that are intrinsically weakly scattering, but imbued with a weak frequency-dependent gain. We study this system using a Green function method [24–28], which includes the coherent retarded electrodynamic coupling between all particles, and radiative damping as the essential ingredient. Contrary to our previous findings on arrays of plasmonic nanoparticles with a shell of gain [29], the scatterers considered here are not resonant by means of localized plasmon or Mie resonances [30] but only due to a spectrally dependent gain medium. While even with gain, each particle is a weak scatterer with response dominated by radiative loss, and their optical response is significantly modified in arrays, where the interplay of gain, loss, and interference gives rise to scattering anomalies. These anomalies resemble sharp resonances associated with lasing thresholds, studied over the past decades in various gain-doped dielectric structures [31–41]. In contrast to these reports, the anomalies discussed in this work result from interference effects caused by gain-induced phase alteration, leading to trapping of light inside the gain medium. Furthermore, by considering the case of a resonant gain, we show that these anomalies must always emerge in pairs, and each of them is surrounded by a phase vortex, producing a scattered field of diverging amplitude and undefined phase, which makes them analogous to phase singularities observed in perfectly absorbing structures [42]. We find that similar anomalies already occur

***Corresponding author: A. Femius Koenderink**, Center for Nanophotonics, AMOLF, Science Park 104, 1098XG Amsterdam, The Netherlands, E-mail: f.koenderink@amolf.nl. https://orcid.org/0000-0003-1617-5748
Radoslaw Kolkowski: Center for Nanophotonics, AMOLF, Science Park 104, 1098XG Amsterdam, The Netherlands. https://orcid.org/0000-0003-3866-9394

in the reflectivity of a prism-coupled gain medium slab, where the incident light couples evanescently to guided modes in a traditional attenuated total reflection setup (Figure 1, right). This divergent coupling to amplified weakly guided slab modes provides an explanation for the metasurface behavior. Similar guided modes are supported by metasurfaces, even composed of weakly polarizable scatterers. Due to periodicity, these are coupled to free space, leading to the observed singularities.

2 Results and discussion

2.1 Scattering by a single nonlasing active nanoparticle

We consider lattices of small spherical nanoparticles (radius $\rho = 80$ nm) that in the absence of gain have a refractive index $n_g = 1.55$, so that they are almost index matched with the passive host medium of index $n_d = 1.5$. In addition, the particles are assumed to have a Lorentzian gain [12] with peak at $\hbar\omega_g = 2.25$ eV, bandwidth $\hbar\gamma_g = 0.025$ eV, and maximum material gain $g_{\max} = 300$ cm^{-1}. The relative permittivity ε_g of such a gain medium is governed by

$$\varepsilon_g = n_g^2\left(1 + g_{\max}\, k_g^{-1}\, \frac{\gamma_g}{\omega_g - \omega + i\gamma_g}\right) \tag{1}$$

where $k_g = n_g\omega_g/c$ is the wave number in the gain medium at the gain peak. In the static limit, the polarizability of this nanoparticle can be expressed as

$$\boldsymbol{\alpha}_{\text{stat}} = \frac{3V}{4\pi}\,\frac{\varepsilon_g - \varepsilon_d}{\varepsilon_g + 2\varepsilon_d}\,\mathbb{I} \tag{2}$$

where $\varepsilon_d = n_d^2$ is the relative permittivity of the surrounding medium, $V = 4\pi\rho^3/3$ is the nanoparticle's volume, and $\mathbb{I}$ is the identity operator. The choice of units in Eq. (2) is the same as in the study by Sersic et al. [10]. Due to the small particle size and low index contrast ($\Delta n = 0.05$), we can safely neglect magnetic, magnetoelectric, and nondipolar effects. The scattering of light is determined by the nanoparticle's dynamic polarizability $\boldsymbol{\alpha}_{\text{dyn}}$, which is obtained from $\boldsymbol{\alpha}_{\text{stat}}$ by adding radiation loss [10, 43, 44]:

$$\boldsymbol{\alpha}_{\text{dyn}}^{-1} = \boldsymbol{\alpha}_{\text{stat}}^{-1} - \frac{2i}{3}k^3\mathbb{I} \tag{3}$$

where $k = n_d\omega/c$ is the wave number in the dielectric environment. The spectral dependence of ε_g, α_{stat}, and α_{dyn} (scalar values on the tensor diagonal) is plotted in Figure 2a and b, respectively.

Previous studies on gain-doped spherical scatterers focused mainly on high-Δn and/or high-gain scenarios, often predicting huge amplification at discrete wavelengths and incidence angles [31, 33] already for single particles. In these cases, extreme optical responses could be attributed to narrowing of the particle's Mie resonances in the vicinity of their lasing thresholds, i.e., near the conditions of their radiative loss compensation [38, 41]. In contrast, our nanoparticles by themselves are only very weakly polarizable and operate in the Rayleigh limit, i.e., away from any intrinsic particle resonances. They cannot by themselves become a laser, as there is no resonance to provide feedback, and furthermore, the assumed gain is by far insufficient to compensate the radiative loss. This is apparent from Figure 2c showing extinction and scattering cross sections of this particle: $\sigma_{\text{ext}} = 4\pi k\,\text{Im}\{\alpha_{\text{dyn}}\}$ and $\sigma_{\text{scat}} = 8\pi k^4|\alpha_{\text{dyn}}|^2/3$, respectively. In the spectral range of gain, $0 < \sigma_{\text{ext}} < \sigma_{\text{scat}}$, meaning that while the nanoparticle slightly attenuates the incoming wave, its total scattered energy is slightly greater than the energy it takes from the beam as extinction. In the next section, we explore the

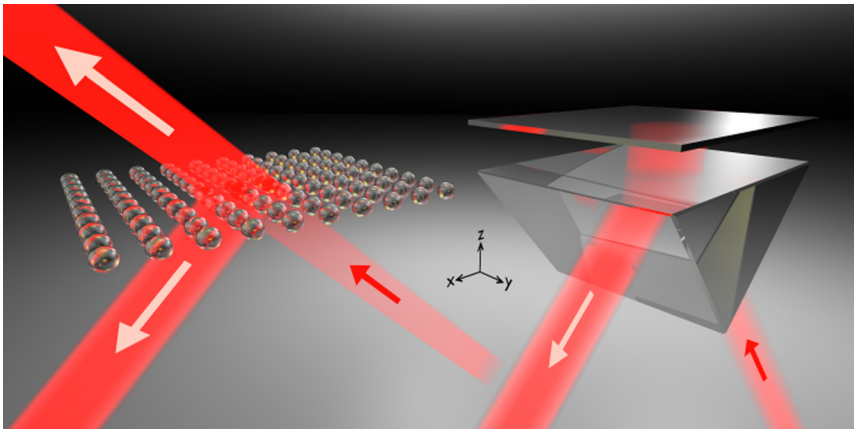

Figure 1: Photonic structures discussed in this work, featuring gain-induced phase singularities in the frequency–momentum space, accompanied by diverging amplitude of the scattering observables.
Left: periodic array of weakly polarizable gain medium nanoparticles has scattering anomalies in transmission and reflection.
Right: prism-coupled gain medium layer shows scattering anomalies in attenuated total internal reflection.

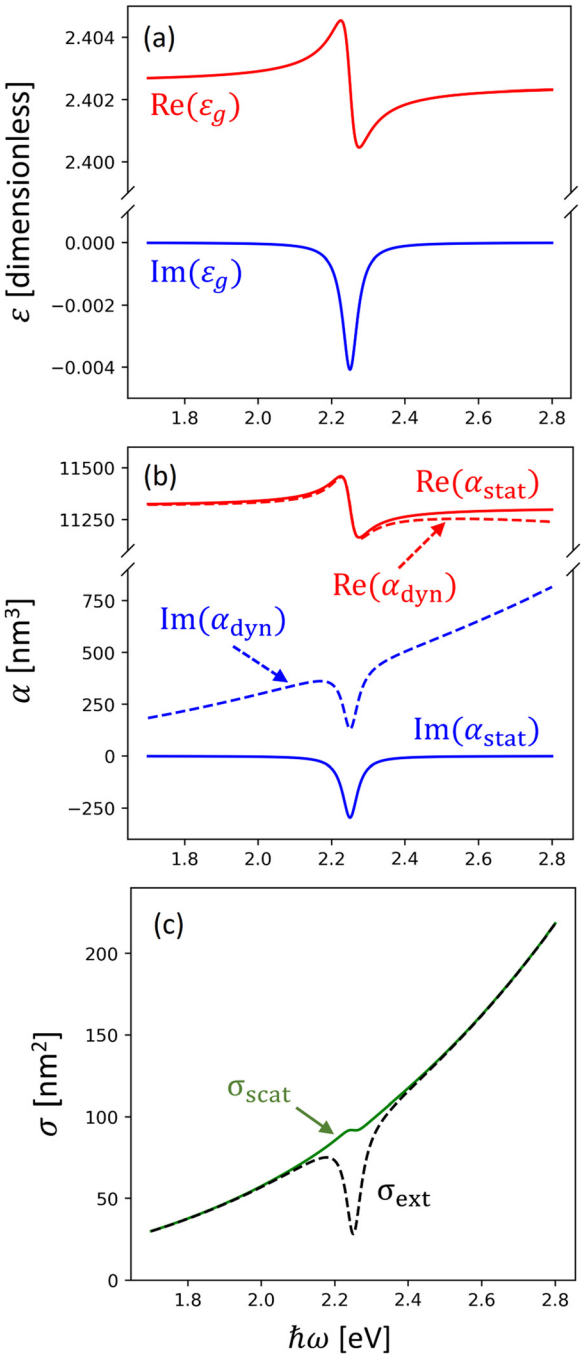

Figure 2: (a) Electric permittivity ε_g of a gain medium with refractive index n_g = 1.55, gain bandwidth $\hbar\gamma_g$ = 0.025 eV, and peak gain coefficient g_{max} = 300 cm^{-1} at $\hbar\omega_g$ = 2.25 eV: real part – red, imaginary part – blue. (b) Scalar polarizabilities α of a gain medium nanoparticle of radius ρ = 80 nm embedded in a dielectric environment of refractive index n_d = 1.5: static polarizability – solid lines, dynamic polarizability – dashed lines, real part – red, imaginary part – blue. (c) Optical cross sections σ of the same nanoparticle: scattering cross section – solid green, extinction cross section – dashed black.

possibility of enhancing the weak individual response of such nanoparticles by their periodic arrangement.

2.2 Scattering by an array of nanoparticles

For periodic arrays under plane wave illumination, Bloch theorem allows to express the lattice-corrected response of each nanoparticle using effective polarizability $\boldsymbol{\alpha}_{\text{eff}}$ [24–29] which depends on the frequency ω and in-plane momentum $\mathbf{k}_{||}$:

$$\mathbf{p}(\omega, \mathbf{k}_{||}) = \boldsymbol{\alpha}_{\text{eff}}(\omega, \mathbf{k}_{||})\mathbf{E}_{\text{inc}}(\omega, \mathbf{k}_{||}) \tag{4}$$

where $\mathbf{p}$ is the induced dipole moment and $\mathbf{E}$ is the incident field, whereas $\boldsymbol{\alpha}_{\text{eff}}$ is obtained from

$$\boldsymbol{\alpha}_{\text{eff}}^{-1}(\omega, \mathbf{k}_{||}) = \boldsymbol{\alpha}_{\text{dyn}}^{-1}(\omega) - \mathcal{G}_{\text{latt}}(\omega, \mathbf{k}_{||}) \tag{5}$$

where $\mathcal{G}_{\text{latt}}$ is the lattice Green function which encodes the electromagnetic interparticle couplings, and $\boldsymbol{\alpha}_{\text{dyn}}$ can be calculated using Eqs. (1)–(3). Details on simulating the optical properties of metasurfaces can be found in the studies by Zou et al [24], de Abajo [25], Lunnemann et al [26], Kwadrin and Koenderink [27], Lunnemann and Koenderink [28], and Kolkowski and Koenderink [29] and in the Supplementary material S1.

Here, we consider the same nanoparticles as in the previous section, arranged into a square array of pitch a = 250 nm. Figure 3 shows the transmissivity and reflectivity of this array under s- and p-polarized illumination (T_s, T_p, R_s, and R_p) as a function of ω and $\mathbf{k}_{||}$. Since the individual nanoparticles are weakly polarizable, the overall optical response of the array is rather weak, with some enhancement near the Rayleigh anomalies, one of which is highlighted by the green dashed line. In the next section, we will show that there are actually hidden singular points of extreme T and R, which are not resolved in Figure 3, but can be revealed by proper magnification of the parameter space.

2.3 Diverging lattice polarizability near the Rayleigh anomaly

Figure 4a–d shows a magnification of Figure 3 around the intersection between the gain band, visible as blue color in Figure 3a and b, and the (1, 0)-Rayleigh anomaly highlighted by the green dashed line. Here, the parameter space is tilted by substituting $k_x a/\pi$ on the horizontal axis by $(k_x + k)a/\pi - 2$, enforcing the alignment of the vertical frequency axis with the (1, 0)-Rayleigh anomaly, and enabling exploration of its closest vicinity. This approach

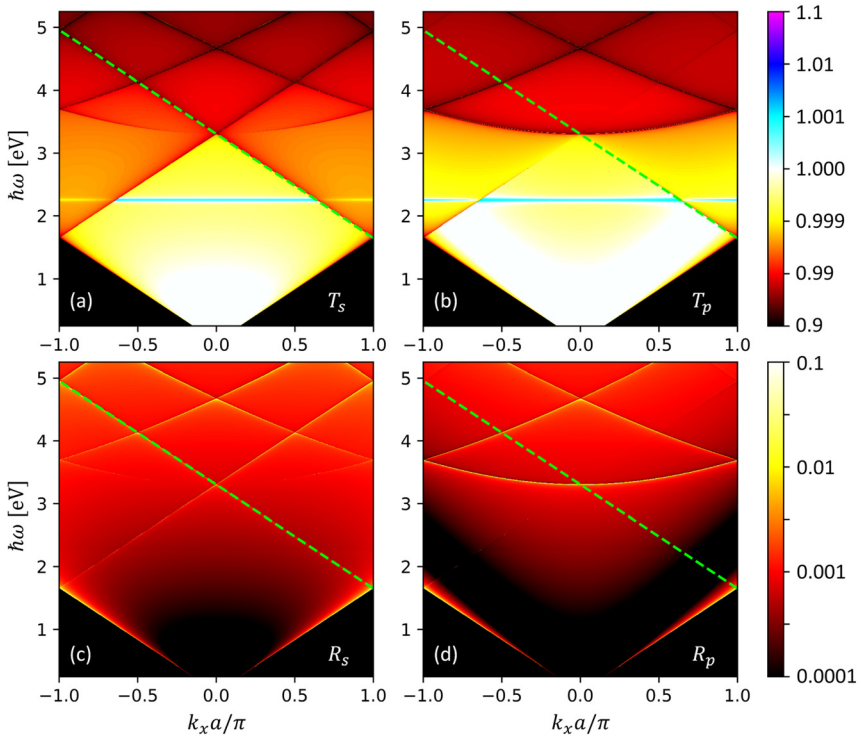

Figure 3: Zero-order transmission and reflection from a square lattice (pitch a = 250 nm, background index n_d = 1.5) of spherical nanoparticles with gain (parameters as in Figure 2), as a function of frequency ω and in-plane momentum k_x (for k_y = 0): (a, b) transmissivity T, (c, d) reflectivity R, for (a, c) s-polarized (TE), and (b, d) p-polarized (TM) incident light. Green dashed lines mark the (1, 0)-Rayleigh anomaly.

reveals a narrow lattice resonance that is excited under both s and p incident polarizations. As seen from Figure 4a–d, this mode "hybridizes" with the frequency-dependent material gain, leading to T and R of at least 10^3, revealed by further zoom into the singularities, presented in the insets. We will prove that T and R are divergent at these points and are associated with a phase singularity in the response.

An effective analysis method of the lattice response is to note that the response tensor for the lattice defined by Eq. (5) can be diagonalized to find eigenvalues (eigenpolarizabilities) and eigenvectors (eigenilluminations). Moreover, the *inverse* lattice polarizability $\boldsymbol{\alpha}_{\mathrm{eff}}^{-1}$ generally shares its eigenvectors with $\boldsymbol{\alpha}_{\mathrm{eff}}$, while the eigenvalues are just the *inverse* eigenpolarizabilities. Therefore, if just one eigenvalue of $\boldsymbol{\alpha}_{\mathrm{eff}}^{-1}$ tends to $0 + 0i$, then at least one eigenvalue of $\boldsymbol{\alpha}_{\mathrm{eff}}$ becomes divergent. This is clearly the case in Figure 4e–g, which shows that the second and the third inverse eigenpolarizability, corresponding to the y-oriented (in plane, transverse to $\mathbf{k}_{||}$) and the z-oriented (out of plane) dipoles, must both have at least two complex zeros. This is evident from the sign-change contours in the real and imaginary parts. The real part is frequency and momentum dependent, while the imaginary part is mostly frequency dependent but with negligible variation along the momentum axis over the magnified range. Hence, the intersection of these contours cannot be avoided. The distribution of $\mathrm{Re}\{\boldsymbol{\alpha}_{\mathrm{eff}}^{-1}\}$ originates from the resonant character of scattering in the vicinity of Rayleigh anomalies, showing *de facto* a dispersive (frequency- and momentum-dependent) lattice mode, which appears inside the light cone due to band folding of the weakly guided metasurface mode. Due to low index contrast, radiative damping has only a moderate contribution to $\mathrm{Im}\{\boldsymbol{\alpha}_{\mathrm{eff}}^{-1}\}$ in the absence of the first-order diffraction (that is, on the left-hand side of the Rayleigh anomaly in Figure 4), and therefore, it is entirely dominated by the frequency-dependent gain band of the nanoparticles material, which does not depend on the in-plane momentum. As seen in Figure 4, this particular distribution leads to diverging T and R at the $\mathbf{k}_{||}$–ω points where the incoming light couples to the corresponding divergent eigenpolarizabities.

Figure 4i–l shows the phase response in reflection and transmission near the points of singular response. Clearly, phase vortices of opposite topological charge appear for the pairs of these points. Here, we define the topological charge as an integral over phase (modulo 2π) along a closed path surrounding a given point in the frequency–momentum plane. The insets in Figure 4i–l show that upon clockwise encirclement of the lower frequency singularity, one would acquire a full 2π phase jump. Encircling the other singularity (the one at higher frequency) would result in a phase jump of -2π. This is a direct consequence of the fact that the eigenpolarizabilities in Figure 4e–h are

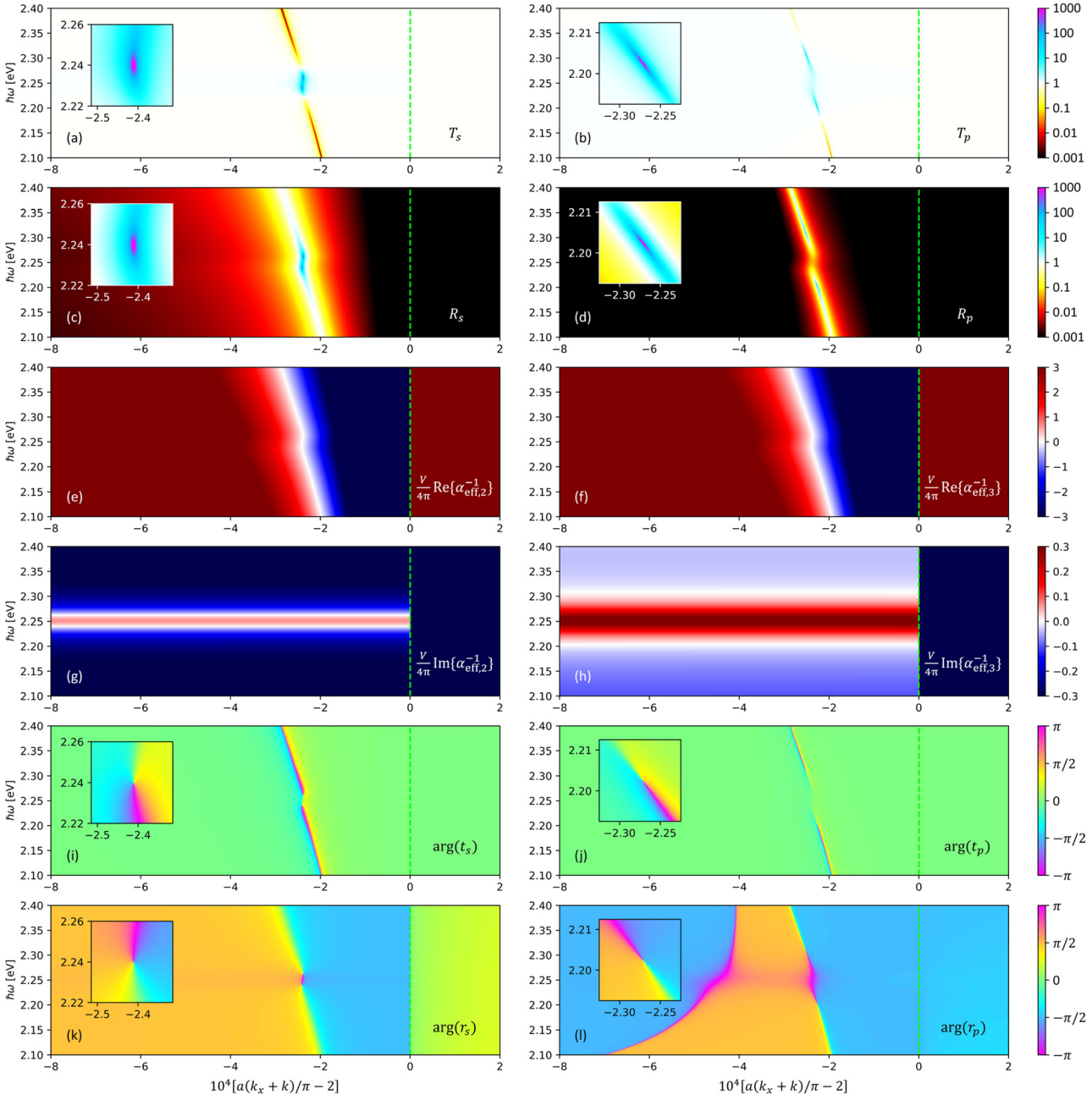

Figure 4: Magnification of Figure 3, with the momentum axis corrected to match with the (1, 0)-Rayleigh anomaly, which now appears vertical and is marked by the green dashed line.
(a, b) Transmissivity, (c, d) reflectivity, for (a, c) s-polarized, and (b, d) p-polarized incident light. (e, f) Real part, and (g, h) imaginary part of (e, g) the second and (f, h) the third eigenvalue of the inverse effective polarizability $\boldsymbol{\alpha}^{-1}_{\mathrm{eff}}$. Positive-zero-negative values are encoded in the red-white-blue color scale. For both eigenvalues, the real part crosses zero along the in-plane momentum axis, whereas the imaginary part crosses zero twice along the frequency axis. The intersections between the real and the imaginary sign-change contours produce pairs of phase vortices with topological charge ±1, which are visible in the phase plots in (i–l), calculated as the argument of the complex transmission/reflection coefficient t and r corresponding to (a–d) ($R = |r|^2$, $T = |t|^2$). The insets show further magnification of the singularities (the ones at lower ω) and their coincidence with centers of phase vortices.

complex functions that show pairs of simple zeros. The scattering phase inside each vortex is undefined, and the vortices can be regarded as counterpart to the singular phase at scattering zeros in perfectly absorbing systems [42]. It is the Lorentzian resonant frequency dependence of the gain that causes the topological charge of each vortex to be ±1 and whereby the singularities must always emerge in oppositely charged pairs (one singularity per each side of the gain band). The singularities annihilate each other once the gain is reduced below a certain threshold. This is

demonstrated in Figure 5a, where R is plotted versus $\mathbf{k}_{||}$ and $g_{\max}$ at a fixed $\omega = \omega_g$, with a sequence of $\mathbf{k}_{||}$–ω plots for various $g_{\max}$ in Figure 5b. For the p-polarized reflected light, we find a threshold of around 56 cm^{-1}, which is significantly lower than for the s-polarized light (~255 cm^{-1}). This can be explained by noting that in-plane and out-of-plane electric dipoles at the given $\mathbf{k}_{||}$ (corresponding to the incidence angle ~27.9°) have significantly different radiative loss rates.

All singularities discussed above have been presented as pairs of isolated points in the k_x–ω plane. However, if one considers the entire frequency–momentum space (k_x, k_y, ω), these singularities would appear as continuous lines, following the edges of Rayleigh anomalies (which have conical shapes in this parameter space). In terms of phase distribution, these pairs of lines would be topologically similar to pairs of screw dislocations of opposite handedness. To better illustrate the true shape of these contours, in the Supplementary material S2 we present T and R in a fixed-frequency crosscut of momentum space (a Fourier image) and an example $k_{||}$–ω crosscut analogous to Figure 4, but not aligned with k_x. It shows that the singularities may persist in different k-space regions, as long as the gain is sufficient to compensate the radiative losses. However, since the radiative damping is momentum dependent, these contours may merge together and annihilate each other at certain points inside the light cone if the gain becomes too small to compensate the loss. Furthermore, a singularity line may also be terminated by simply decoupling from the far field due to symmetry.

2.4 Singular response of simple weakly amplifying slab waveguides in total reflection

Here, we show that the gain-induced anomalies that we report can even be realized in a system without periodic

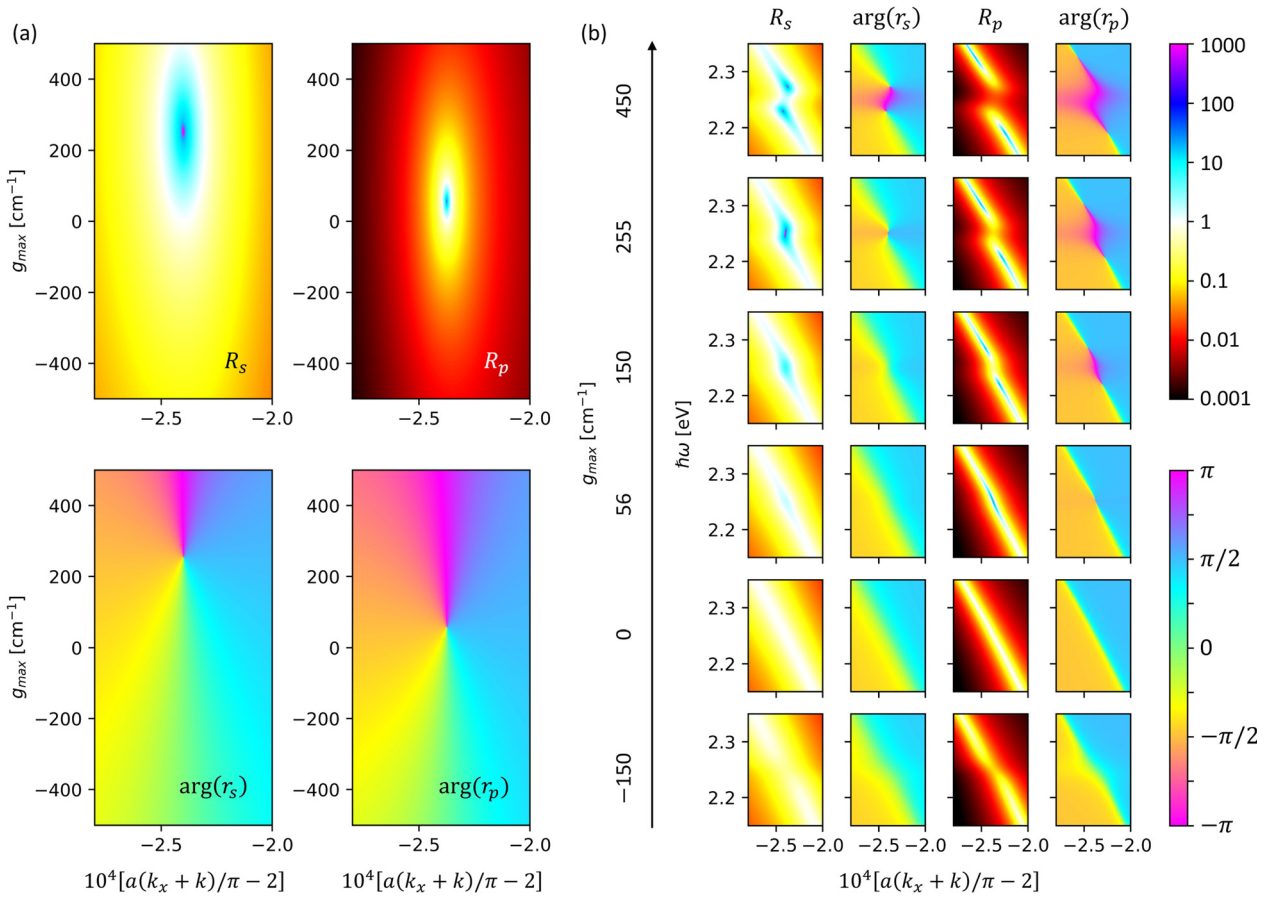

Figure 5: Reflection from a metasurface with either gain or loss.
(a) Dependence of the reflectivity $R_{s,p}$ and the reflected phase $\arg(r_{s,p})$ on the in-plane momentum k_x (horizontal axis) and on the gain coefficient $g_{\max}$ (vertical axis) at a fixed photon energy 2.25 eV. Negative $g_{\max}$ means an effective loss. (b) Frequency–momentum distributions of $R_{s,p}$ and $\arg(r_{s,p})$ at various $g_{\max}$, showing the birth of singularities at ~255 cm^{-1} for the s-polarized light and ~56 cm^{-1} for the p-polarized light.

structuring, namely, in a prism-coupled weakly waveguiding layer with a small amount of optical gain. In the past, there have been several proposals of slab amplifiers [35–37], relying on the interaction of amplified leaky modes with free-space radiation. In contrast, our structure is based on evanescent coupling to a waveguide with gain in attenuated total reflection. This evanescent coupling makes the scenario similar to evanescent lasers [45–49], except that it avoids the branch cut ambiguity [50] by confining the gain medium to a layer of limited thickness. (In our case, the calculated results are independent on the branch cut choice.)

To find parameters that would make a homogeneous gain medium layer similar to the metasurface studied in the previous section, one would need to assign a thickness and a slab dielectric constant according to a homogenization procedure [51]. One approach is to estimate the permittivity ε_l from the particle polarizability and for an assumed slab thickness h according to Clausius–Mossotti relation:

$$\frac{\varepsilon_l - \varepsilon_d}{\varepsilon_l + 2\varepsilon_d} = \frac{4\pi\varepsilon_d}{3} N\alpha_{\text{stat}} \tag{6}$$

where $N = 1/(ha^2)$ is the number density of the nanoparticles. The magnitude of ε_l and its spectral variation depends on the assumed layer thickness h, with exact coincidence between the values of ε_l and ε_g at $h = \varepsilon_d V/a^2 \approx 77.2$ nm (coincidentally very close to $\rho = 80$ nm). Inspired by this reasonable correspondence, we calculate the complex-valued effective mode index n_{eff} of an isolated gain medium layer (in the absence of a prism coupler, in a homogeneous medium of $n = 1.5$) using a transfer matrix approach [52], which is briefly presented in the Supplementary material S3. Figure 6a shows the dispersion of $\text{Re}\{n_{\text{eff}}\}$ for the Transverse Electric (TE) and Transverse Magnetic (TM) guided modes (corresponding to the s and p polarizations, respectively) assuming $h = 80$ nm, and taking ε_l as per the homogenization approach. The modal gain coefficient $g_{\text{mod}} = 2k_0\text{Im}\{n_{\text{eff}}\}$ is encoded in color. Evidently, we are dealing with a very weakly waveguiding slab (mode index of order 1.5015, relative to cladding $n = 1.5$), with a weak modal gain (15 cm^{-1}). Figure 6b shows that the magnitude of n_{eff} depends somewhat on the choice of h, indicating that a 2D array of polarizable particles cannot be strictly homogenized as a dielectric slab. Furthermore, our metasurface does not qualify for the effective medium approximation, since its lattice period is not significantly smaller than the spatial variation of the incident field due to $\mathbf{k}_{||}$. However, we emphasize that the purpose of introducing a gain medium slab in this work is not because we claim that it can closely approximate the metasurface but rather it is to present a simpler system of similar material parameters which exhibits the same kind of singular scattering response. We note that this kind of response occurs irrespective of the precise choice of h used in the homogenization.

Next, we consider coupling of incident light to the envisioned weakly amplifying waveguide by a prism coupler. To this end, we add another interface with a high-index prism medium ($n = 1.75$), spaced from the amplifying slab by a layer of thickness d and index 1.5. As in the previous calculation, the amplifying layer has a thickness $h = 80$ nm and $\varepsilon_l \approx \varepsilon_g$ and is covered by an $n = 1.5$ cladding. We calculate R for the plane waves incident from the high-index prism, expecting to see total internal reflection ($R = 1$) except when matching the waveguide mode in wave vector and frequency. The evanescent coupling introduces a leakage loss to the waveguide mode which depends on the distance d between the prism and the layer. At $d = 2\,\mu$m, we discover points of huge amplification in the regime of total internal reflection just above the critical angle θ_{cr}, shown in

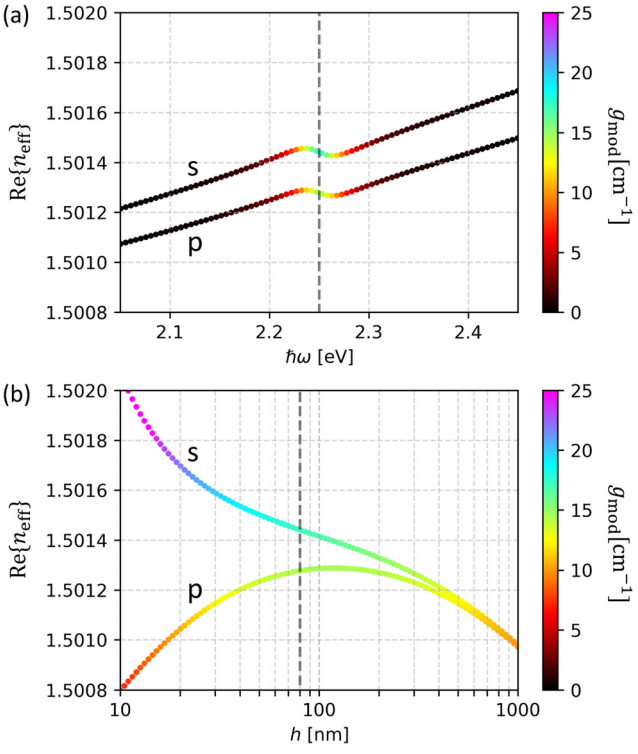

Figure 6: (a) Complex effective mode index n_{eff} calculated using transfer matrix method, for the s- and p-polarized fundamental guided modes of a gain-doped layer that imitates the nanoparticle array from Section 2.3. The layer has permittivity $\varepsilon_l \approx \varepsilon_g$ and thickness $h = 80$ nm and is surrounded by a medium of index $n_d = 1.5$. The gray dashed line marks $\hbar\omega = 2.25$ eV. (b) Dependence of n_{eff} on the assumed h at a fixed photon energy equal to $\hbar\omega_g = 2.25$ eV, with ε_l governed by Eq. (6). The gray dashed line marks $h = 80$ nm. In both (a) and (b), modal gain coefficient $g_{\text{mod}} = 2k_0\text{Im}\{n_{\text{eff}}\}$ is encoded in the color.

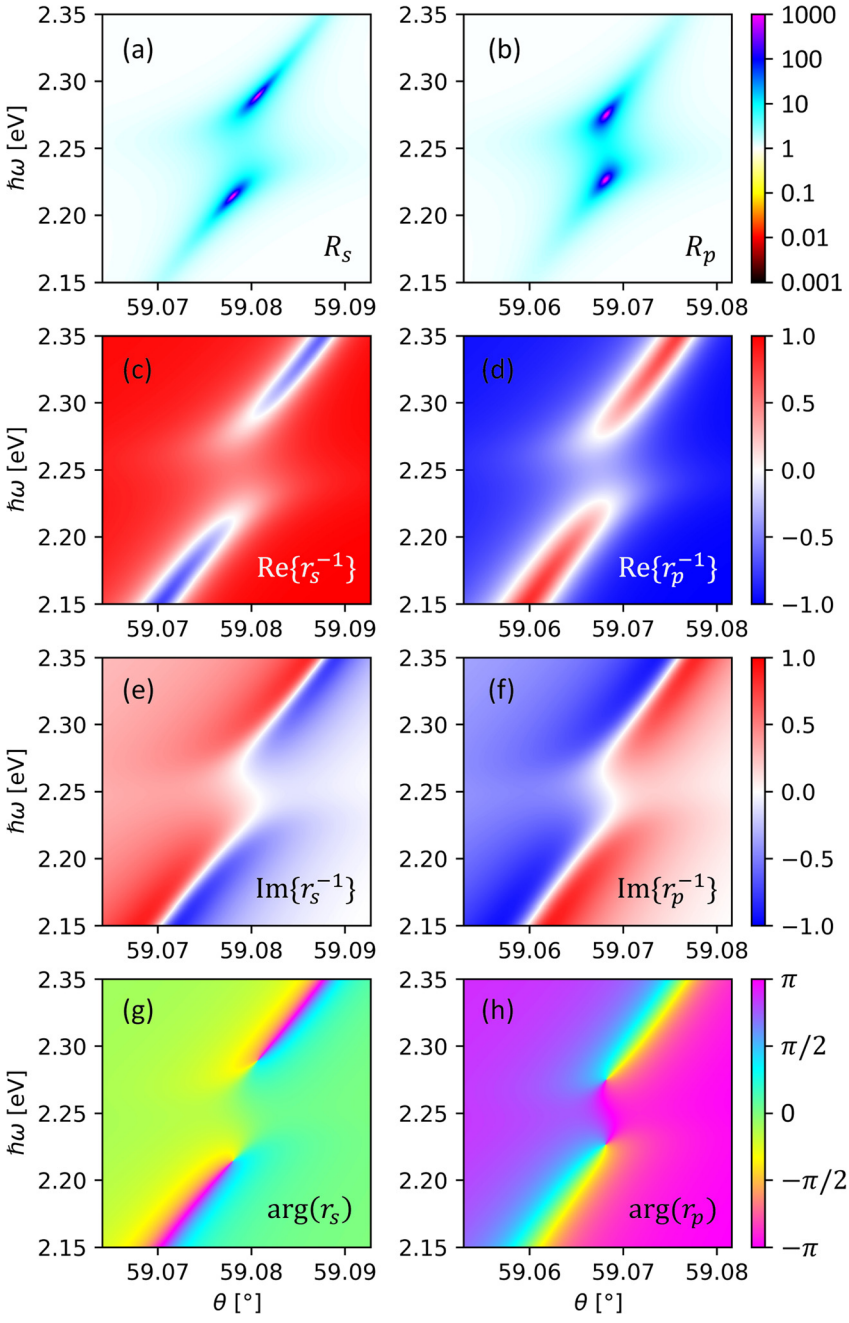

Figure 7: Results of the transfer matrix calculations, showing the amplified reflection just above the critical angle (θ_{cr} = 59.00°) resulting from evanescent coupling of incident light to the guided modes supported by the gain-doped layer as a function of the incidence angle θ and frequency ω, assuming h = 80 nm ($\varepsilon_l \approx \varepsilon_g$), prism index of 1.75, and prism-to-slab distance of 2000 nm. (a, b) Reflectivity R for the s- and p-polarized incident light. (c–f) Distribution of the real and the imaginary part of r^{-1} (inverse of the reflection coefficient). The intersections of the real and the imaginary zeros create pairs of singularities, similar to those observed in Figure 4. (g, h) Pairs of phase vortices with topological charge ±1 coincide with the singularities in (a, b), just like in Figure 4.

Figure 7a and b for both s and p incident polarization, resulting from the intersections of the real and the imaginary sign-change contours in r^{-1} shown in Figure 7c–f. The distribution of the complex-valued reflection coefficient r around these points features pairs of phase vortices, shown in Figure 7g and h, similar to the vortices observed in Figure 4e–h. In the full frequency–momentum space (k_x–k_y–ω), each of these singularies would appear as a ring due to full rotational invariance of the slab, as opposed to periodic metasurfaces, where the singularities are aligned with the edges of Rayleigh anomalies. Furthermore, as opposed to simple metasurfaces in a symmetric host [53], the proposed asymmetric multilayer geometry can also support phase singularities in the lossy regime, which is shown in Figure 8 (analogous to Figure 5). In case of a lossy waveguide, phase singularities become points of perfect absorption (zero in R, and lack of T due to evanescence), similar to those reported in the study by Berkhout and Koenderink [42].

From the above results, we conclude that the singular scattering response of weakly scattering and amplifying metasurfaces is not due to their periodic patterning *per se*.

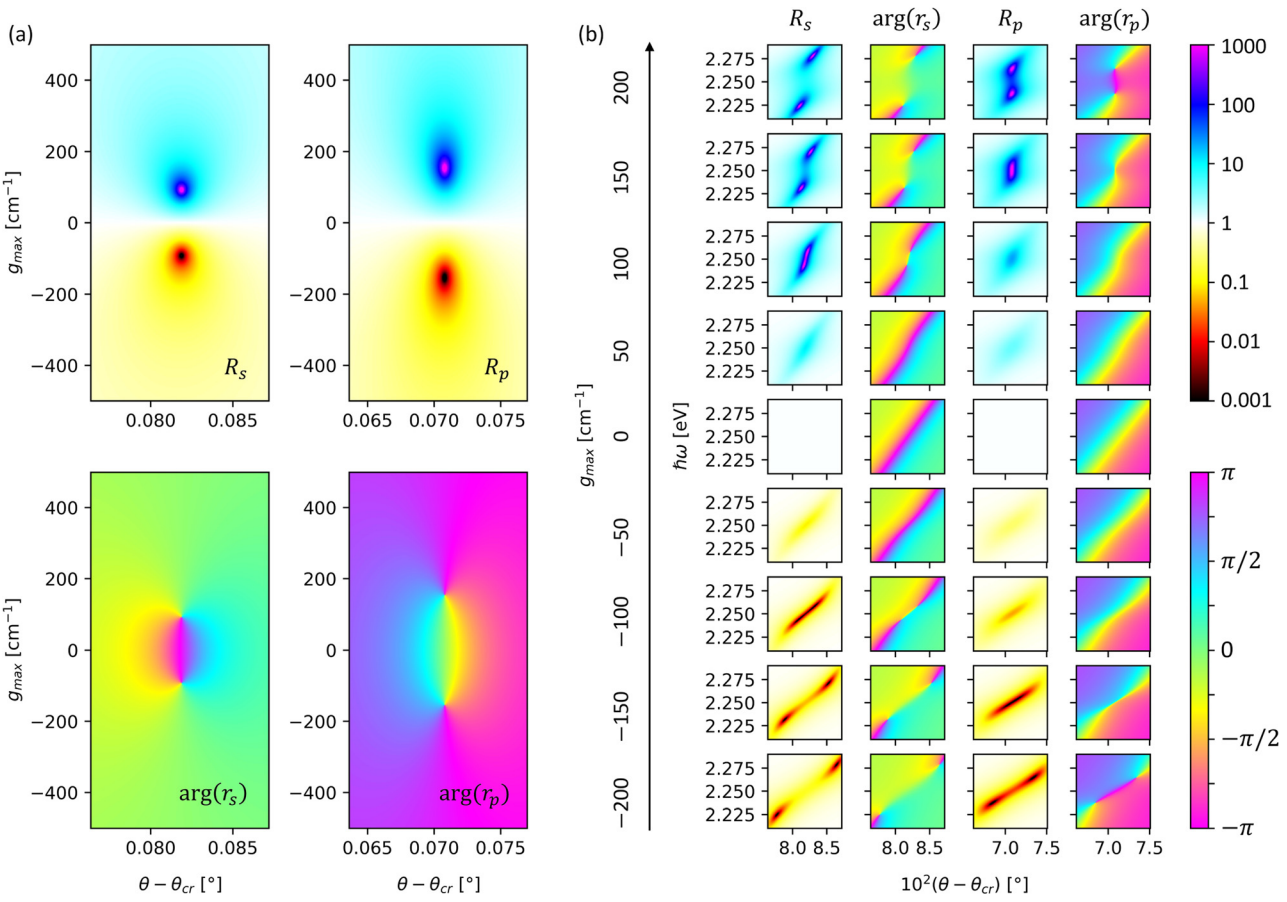

Figure 8: Total internal reflection with evanescent coupling to a thin layer with either gain or loss. (a) Dependence of the reflectivity $R_{s,p}$ and the reflected phase $\arg(r_{s,p})$ on the incidence angle θ (horizontal axis) and on the gain coefficient g_{max} (vertical axis) at a fixed photon energy of 2.25 eV. Negative g_{max} means an effective loss. (b) Frequency–momentum distributions of $R_{s,p}$ and $\arg(r_{s,p})$ at various g_{max}, showing the birth of singularities in the regime of both gain (divergent amplification) and loss (perfect absorption).

In a gain-doped metasurface, the role of periodicity is to act as a grating coupler, folding the guided modes into the light cone and opening a radiative decay channel, which is associated with loss that contributes to the effect of gain on the amplitude and phase of light, leading to the observed anomalies.

2.5 Classification of the scattering anomalies

For better understanding of the anomalies reported here, it is useful to place them among the known scattering phenomena. Krasnok *et al.* [14] have recently provided a thorough classification of diverse scattering anomalies on the basis of zeros and poles in the S-matrix Hamiltonians and scattering coefficients, using the notion of complex eigenfrequencies rather than complex eigenpolarizabilities. The divergence of scattering coefficients presented in our work corresponds exactly to the scenario in which a pole in the scattering coefficient intersects with the real frequency axis due to the balance between the gain of the system's eigenmode and its outcoupling loss. Figure 9 presents the trajectories of such poles obtained using transfer matrix method for the same type of geometry as considered in Section 2.4 – that is, a gain medium slab with and without the coupling prism – taking complex-valued frequencies and real-valued parallel momenta as an input. An isolated gain medium layer supports fundamental TE (s) and TM (p) guided modes with negative imaginary eigenfrequencies (i.e. with net gain). The presence of a coupling prism introduces additional losses, pulling the imaginary eigenfrequencies toward positive values and forcing them to cross zero at singular points in the $k_{||}$ – Re$\{\omega\}$ plane (black circles in Figure 9). Similar behavior can be shown for the eigenfrequencies of a gain medium metasurface discussed in Sections 2.2 and 2.3. To avoid issues with the lattice Green function method (Ewald summations at complex

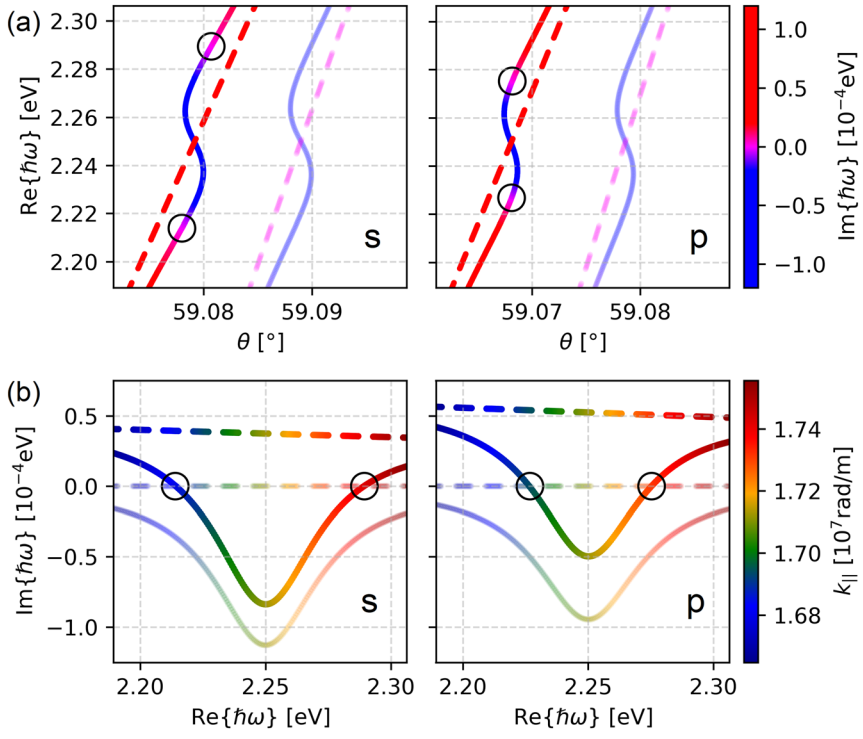

Figure 9: Results of the complex eigenfrequency analysis using transfer matrix method for the gain medium slab waveguide – the same as in Section 2.4 – with the coupling prism (opaque contours/intense colors) and without the coupling prism (semitransparent contours/faint colors): trajectories of the poles of the reflection coefficient as a function of the in-plane momentum $k_{||}$, or incidence angle $\theta = \arcsin(k_{||}k_0^{-1}n_p^{-1})$, and complex-valued frequency ω, corresponding to the TE (s-polarized) and TM (p-polarized) guided modes. Solid contours: $g_{max} = 300$ cm^{-1}, dashed contours: $g_{max} = 0$.(a) Dependence of real eigenfrequencies on the incidence angle, with the imaginary eigenfrequencies encoded in the color (blue = gain, red = loss, magenta = purely real eigenmode). (b) Pole trajectories in the complex frequency plane, with in-plane momentum encoded in the color. In both (a) and (b), black circles mark the intersections of pole trajectories with the real frequency axis. These points correspond to the singularities observed in Figure 7.

frequency), we turn to the commercial full-wave finite-element software COMSOL Multiphysics. COMSOL allows finding the complex eigenfrequencies of our metasurface at real parallel momentum defined by Floquet periodic boundary conditions (see Supplementary material S4 for more details on simulation and the required boundary conditions). Results of these simulations are presented in Figure 10. These results show excellent agreement with Figure 4, confirming the coincidence between the singularities and the intersections of eigenfrequency trajectories with the real ω axis. Moreover, these results are very similar to the results shown in Figure 9, which is another piece of strong evidence that the gain medium metasurface is indeed analogous to the prism-coupled gain medium slab, and their scattering anomalies are manifestations of the same physical mechanism stemming from the interplay between the eigenmode's gain and the outcoupling loss. According to Krasnok et al [14], this scenario corresponds to the scattering behavior of a laser with anomaly occurring at the lasing threshold. Certainly, the role of resonant outcoupling loss in photonic structures discussed in our work is reminiscent of the proposal of Nechepurenko [54] which addresses the emergence of lasing induced by resonant loss in a system with gain.

Nonetheless, there is a remarkable difference between the usual lasing threshold anomalies and the anomalies discussed in our work. In the usual laser, the light is already trapped inside a cavity, such that the net amplification will always diverge (up to gain saturation) above the lasing threshold, as a result of gain accumulated during multiple round trips. In our case, the trapping of light is caused by the gain (or by loss) itself and there is no cavity or distributed feedback. Both gain and loss contribute to the phase acquired by light, and this additional phase leads to interference that can store the light inside the gain medium for a very long time. During such extended scattering event, the constant leakage of light is perfectly balanced by the amplification, such that the total amount of energy carried away by the reflected or transmitted light becomes divergent. A similar mechanism is realized in the evanescently coupled lossy waveguide, where a certain amount of loss leads to coherent trapping of light, which leads to what is known as coherent perfect absorption [55, 56]. In contrast to the usual physics of a laser, excessive gain (or excessive loss) disturbs the scattered phase, such that the divergence is removed. Indeed, the amplification (extinction) at frequencies in between the singularities is significantly weaker, in spite of higher gain (higher loss) in this range. Similar behavior has been achieved by active systems with exceptional points (EPs) [57, 58]; however, in our case, it is shown in much simpler systems, without any use of PT symmetry physics.

Finally, we would like to emphasize that the scattering anomalies presented in this work are not EPs, as the latter ones require at least two complex eigenmodes that are coupled together and form two phases (PT symmetric and

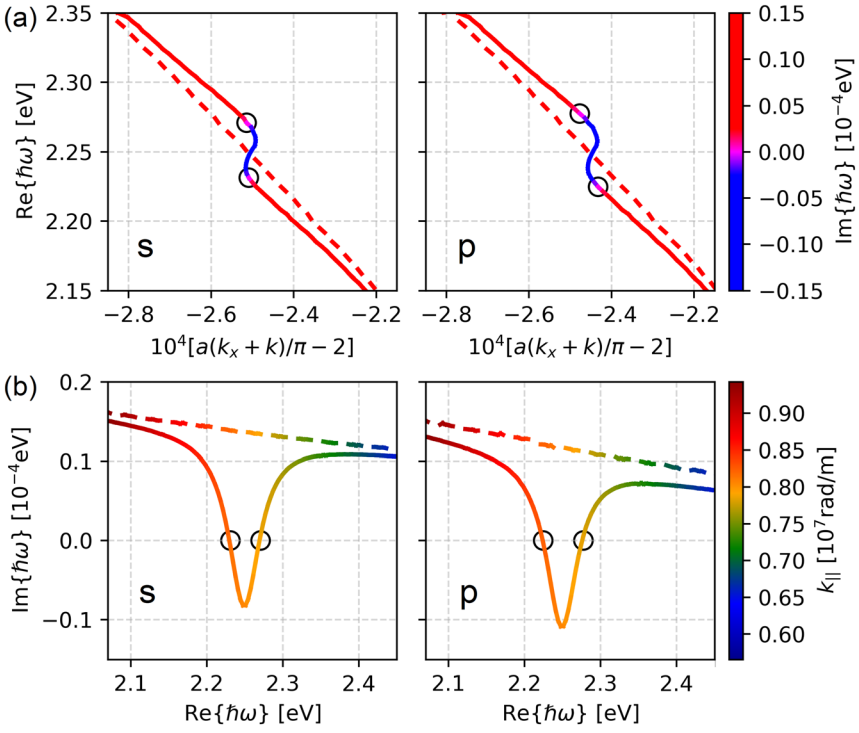

Figure 10: Results of the complex eigenfrequency analysis using finite element method (COMSOL) for periodic metasurface of gain medium nanoparticles – the same as in Sections 2.2 and 2.3: trajectories of the complex-valued eigenfrequencies as a function of k_x, corresponding to the TE (s-polarized/in-plane-oriented dipoles) and TM guided modes (p-polarized/out-of-plane-oriented dipoles). Solid contours: $g_{max} = 300\ \mathrm{cm}^{-1}$, dashed contours: $g_{max} = 0$. (a) Real eigenfrequencies as a function of the in-plane momentum corrected by the Rayleigh anomaly tilt (as in Figure 4), with the imaginary eigenfrequencies encoded in the color (blue = gain, red = loss, magenta = purely real eigenmode). (b) Eigenvalue trajectories in the complex frequency plane, with in-plane momentum encoded in the color. In both (a) and (b), black circles mark the intersections of eigenfrequencies with the real frequency axis. These points correspond to the singularities observed in Figure 4.

with broken PT symmetry) across the parameter space. Generally catastrophic scattering anomalies do not require two complex eigenmodes and hence are distinct from EPs [14, 29]. EPs will only coincide with such anomalies in highly accidental cases, i.e., when gain and loss of two coupled eigenmodes are perfectly balanced in their PT-symmetric phase. This kind of scenario leads to what is referred to as "spectral singularities" [59] and "photonic catastrophe" [60]. EPs may also exist without gain, leading to moderate scattering coefficients [61, 62]. Our gain-doped metasurface cannot support EPs, at least in the $\mathbf{k}_{||}$–ω range under consideration, as there is no coupling between the existing eigenmodes (ensured by the assumption of isotropic spherical scatterers, square lattice with one particle per unit cell, as well as the absence of magnetoelectric or multipolar effects). On the other hand, our system could exhibit EPs in other regions of the $\mathbf{k}_{||}$–ω space, for instance, near the intersection of Rayleigh anomalies where two or more copies of the same eigenmode could interact in a non-Hermitian manner [19]. This is certainly an exciting target for further exploration of such metasurfaces.

3 Conclusions and outlook

We have shown that periodic arrays of weakly polarizable scatterers can support scattering anomalies accompanied by phase vortices. The main challenge in observing these singular features in experiments comes from the assumptions that the array and the incident plane wave are significantly extended in space and time, such that their frequency–momentum distributions are nearly Dirac deltas. In a real system, the singularities would be blurred due to finite size of the illuminated area [37, 63], and due to finite time duration of the scattering events, especially in a pulsed pump-probe implementation [64, 65]. Large amplification requires that each incoming photon is scattered and amplified many times by many nanoparticles, in a way resembling amplification in a resonant cavity [66], which may take a long time to build up. In that context, practical limitations may arise from the inherent properties of real systems, with their transient dynamics, saturation, optical breakdown, and spontaneous decay [21, 22].

Fortunately, many of these constraints can be relaxed by developing new materials (gain media with slow population dynamics) and by design of the experiment, including fabrication of large-area metasurfaces and implementation of an appropriate time-resolved technique. Since the proposed metasurfaces are based on nonresonant all-dielectric building blocks with moderate material gain, their realization should be technically less challenging compared to most of the proposed high-gain resonant devices [67].

We believe that our theoretical predictions could be useful for designing ultrathin amplifiers and light-emitting devices operating close to the normal incidence, with

particular interest in the dynamic control of the scattered amplitude and phase, e.g., beam steering by metasurfaces with nonuniform gain, or with operation principles similar to the proposed active plasmonic devices [68]. Diverging effective polarizability can also be used for enhancing various light–matter interactions, such as spontaneous emission (Purcell effect), back action, strong coupling, and optical nonlinearities. A prism-coupled slab geometry discussed in Section 2.4 could be an elegant starting point for the experimental demonstration of the proposed mechanisms.

Acknowledgement: This work was performed at the research institute AMOLF, as part of the research program Hybrid Nanophotonic Architectures for Ultrafast Quantum Optics with project number 680.47.621 and of the research program Nanophotonics for Solid-State Lighting with project number Project FOM-i33/680.93.33, which are both (partly) financed by the Dutch Research Council (NWO).
Author contribution: All the authors have accepted responsibility for the entire content of this submitted manuscript and approved submission.
Research funding: The authors acknowledge the financial support of the Dutch Research Council (NWO).
Conflict of interest statement: The authors declare no conflicts of interest regarding this article.

References

[1] N. Yu, P. Genevet, M. A. Kats, et al., "Light propagation with phase discontinuities: generalized laws of reflection and refraction," *Science*, vol. 334, no. 6054, pp. 333–337, 2011.
[2] N. Yu and F. Capasso, "Flat optics with designer metasurfaces," *Nat. Mater.*, vol. 13, pp. 139–150, 2014.
[3] A. Silva, F. Monticone, G. Castaldi, V. Galdi, A. Alù, and N. Engheta, "Performing mathematical operations with metamaterials," *Science*, vol. 343, no. 6167, pp. 160–163, 2014.
[4] S. B. Glybovski, S. A. Tretyakov, P. A. Belov, Y. S. Kivshar, and C. R. Simovski, "Metasurfaces: from microwaves to visible," *Phys. Rep.*, vol. 634, pp. 1–72, 2016.
[5] A. Vaskin, R. Kolkowski, A. F. Koenderink, and I. Staude, "Light-emitting metasurfaces," *Nanophotonics*, vol. 8, no. 7, pp. 1151–1198, 2019.
[6] D. Wang, W. Wang, M. P. Knudson, G. C. Schatz, and T. W. Odom, "Structural engineering in plasmon nanolasers," *Chem. Rev.*, vol. 118, no. 6, pp. 2865–2881, 2017.
[7] V. G. Kravets, A. V. Kabashin, W. L. Barnes, and A. N. Grigorenko, "Plasmonic surface lattice resonances: a review of properties and applications," *Chem. Rev.*, vol. 118, no. 12, pp. 5912–5951, 2018.
[8] M. Greenberg and M. Orenstein, "Irreversible coupling by use of dissipative optics," *Optics Lett.*, vol. 29, no. 5, pp. 451–453, 2004.
[9] N. M. Estakhri and A. Alù, "Wave-front transformation with gradient metasurfaces," *Phys. Rev. X*, vol. 6, no. 4, 2016, Art no. 041008.
[10] I. Sersic, C. Tuambilangana, T. Kampfrath, and A. F. Koenderink, "Magnetoelectric point scattering theory for metamaterial scatterers," *Phys. Rev. B*, vol. 83, p. 245102, 2011.
[11] I. Sersic, M. A. van de Haar, F. B. Arango, and A. F. Koenderink, "Ubiquity of optical activity in planar metamaterial scatterers," *Phys. Rev. Lett.*, vol. 108, p. 223903, 2012.
[12] A. Manjavacas, "Anisotropic optical response of nanostructures with balanced gain and loss," *ACS Photonics*, vol. 3, no. 7, pp. 1301–1307, 2016.
[13] S. Sanders and A. Manjavacas, "Nanoantennas with balanced gain and loss," *Nanophotonics*, vol. 9, no. 2, pp. 473–480, 2020.
[14] A. Krasnok, D. Baranov, H. Li, M. A. Miri, F. Monticone, and A. Alú, "Anomalies in light scattering," *Adv. Opt. Photon.*, vol. 11, no. 4, pp. 892–951, 2019.
[15] C. Ling, K. H. Choi, T. Mok, Z. Q. Zhang, and K. H. Fung, "Anomalous light scattering by topological PT-symmetric particle arrays," *Sci. Rep.*, vol. 6, p. 38049, 2016.
[16] S. Feng, "Loss-induced super scattering and gain-induced absorption," *Optic Express*, vol. 24, no. 2, pp. 1291–1304, 2016.
[17] M. A. Miri and A. Alù, "Exceptional points in optics and photonics," *Science*, vol. 363, p. eaar7709, 2019.
[18] T. D. Visser, H. Blok, and D. Lenstra, "Modal analysis of a planar waveguide with gain and losses," *IEEE J. Quantum Electron.*, vol. 31, no. 10, pp. 1803–1810, 1995.
[19] A. Cerjan, A. Raman, and S. Fan, "Exceptional contours and band structure design in parity-time symmetric photonic crystals," *Phys. Rev. Lett.*, vol. 116, no. 20, p. 203902, 2016.
[20] F. Monticone, C. A. Valagiannopoulos, and A. Alù, "Parity-time symmetric nonlocal metasurfaces: all-angle negative refraction and volumetric imaging," *Phys. Rev. X*, vol. 6, no. 4, 2016, Art no. 041018.
[21] H. Schomerus, "Quantum noise and self-sustained radiation of PT-symmetric systems," *Phys. Rev. Lett.*, vol. 104, p. 233601, 2010.
[22] Y. D. Chong, L. Ge, and A. D. Stone, "PT-symmetry breaking and laser-absorber modes in optical scattering systems," *Phys. Rev. Lett.*, vol. 106, 2011, Art no. 093902.
[23] A. Pick, B. Zhen, O. D. Miller, et al., "General theory of spontaneous emission near exceptional points," *Opt Exp.*, vol. 25, no. 11, pp. 12325–12348, 2017.
[24] S. Zou, N. Janel, and G. C. Schatz, "Silver nanoparticle array structures that produce remarkably narrow plasmon lineshapes," *J. Chem. Phys.*, vol. 120, p. 10871, 2004.
[25] F. J. G. de Abajo, "Colloquium: light scattering by particle and hole arrays," *Rev. Mod. Phys.*, vol. 79, p. 1267, 2007.
[26] P. Lunnemann, I. Sersic, and A. F. Koenderink, "Optical properties of two-dimensional magnetoelectric point scattering lattices," *Phys. Rev. B*, vol. 88, p. 245109, 2013.
[27] A. Kwadrin and A. F. Koenderink, "Diffractive stacks of metamaterial lattices with a complex unit cell: self-consistent long-range bianisotropic interactions in experiment and theory," *Phys. Rev. B*, vol. 89, 2014, Art no. 045120.
[28] P. Lunnemann and A. F. Koenderink, "Dispersion of guided modes in two-dimensional split ring lattices," *Phys. Rev. B*, vol. 90, p. 245416, 2014.

[29] R. Kolkowski and F. Koenderink, "Lattice resonances in optical metasurfaces with gain and loss," *Proc. IEEE*, vol. 108, no. 5, pp. 795–818, 2019.
[30] A. I. Kuznetsov, A. E. Miroshnichenko, M. L. Brongersma, Y. S. Kivshar, and B. Lukyanchuk, "Optically resonant dielectric nanostructures," *Science*, vol. 354, no. 6314, aag2472, 2016.
[31] N. G. Alexopoulos and N. K. Uzunoglu, "Electromagnetic scattering from active objects: invisible scatterers," *Appl. Optics*, vol. 17, no. 2, pp. 235–239, 1978.
[32] M. Kerker, "Electromagnetic scattering from active objects," *Appl. Optics*, vol. 17, no. 21, pp. 3337–3339, 1978.
[33] M. Kerker, "Resonances in electromagnetic scattering by objects with negative absorption," *Appl. Optics*, vol. 18, no. 8, pp. 1180–1189, 1979.
[34] A. Cohen, "Reflection coefficients of large active scatterers," *J. Appl. Phys.*, vol. 58, p. 2437, 1985.
[35] S. N. Mendenhall, O. M. Stafsudd, and N. G. Alexopoulos, "Resonant optical interactions in active dielectric films," *J. Appl. Phys.*, vol. 66, p. 4645, 1989.
[36] S. N. Mendenhall, O. M. Stafsudd, and N. G. Alexopoulos, "Phase-matched electromagnetic scattering in active dielectric films," *Optics Lett.*, vol. 14, no. 21, pp. 1234–1236, 1989.
[37] M. J. Halmos and O. M. Stafsudd, "Dielectric film optical amplifier," *Appl. Optics*, vol. 29, no. 18, pp. 2760–2768, 1990.
[38] S. S. Yi and O. M. Stafsudd, "Observation of lossless radiative modes of a dielectric sphere," *J. Appl. Phys.*, vol. 86, p. 3694, 1999.
[39] S. S. Yi, "Asymptotic analysis of active scattering resonances for large spheres," *Optic Commun.*, vol. 159, pp. 7–12, 1999.
[40] S. S. Yi, "Observation of the resonant optical interactions in active dielectric cylinder," *J. Appl. Phys.*, vol. 87, p. 2090, 2000.
[41] K. L. van der Molen, P. Zijlstra, A. Lagendijk, and A. P. Mosk, "Laser threshold of Mie resonances," *Optics Lett.*, vol. 31, no. 10, pp. 1432–1434, 2006.
[42] A. Berkhout and A. F. Koenderink, "Perfect absorption and phase singularities in plasmon antenna array etalons," *ACS Photonics*, vol. 6, no. 11, pp. 2917–2925, 2019.
[43] A. Lagendijk and B. A. van Tiggelen, "Resonant multiple scattering of light," *Phys. Rep.*, vol. 270, no. 3, pp. 143–215, 1996.
[44] P. de Vries, D. V. van Coevorden, and A. Lagendijk, "Point scatterers for classical waves," *Rev. Mod. Phys.*, vol. 70, no. 2, pp. 447–466, 1998.
[45] C. Koester, "Laser action by enhanced total internal reflection," *IEEE J. Quant. Electron.*, vol. 2, no. 9, pp. 580–584, 1966.
[46] E. Ippen and C. Shank, "Evanescent-field-pumped dye laser," *Appl. Phys. Lett.*, vol. 21, no. 7, pp. 301–302, 1972.
[47] X. Jiang, Q. Song, L. Xu, J. Fu, and L. Tong, "Microfiber knot dye laser based on the evanescent-wave-coupled gain," *Appl. Phys. Lett.*, vol. 90, no. 23, p. 233501, 2007.
[48] H. J. Moon, Y. T. Chough, and K. An, "Cylindrical microcavity laser based on the evanescent-wave-coupled gain," *Phys. Rev. Lett.*, vol. 85, no. 15, p. 3161, 2000.
[49] A. W. Fang, H. Park, O. Cohen, R. Jones, M. J. Paniccia, and J. E. Bowers, "Electrically pumped hybrid AlGaInAs-silicon evanescent laser," *Optic Express*, vol. 14, no. 20, pp. 9203–9210, 2006.
[50] A. Siegman, "Fresnel reflection, lenserf reflection and evanescent gain," *Optic Photon. News*, vol. 21, no. 1, pp. 38–45, 2010.
[51] Y. Zhao, N. Engheta, and A. Alù, "Homogenization of plasmonic metasurfaces modeled as transmission-line loads," *Metamaterials*, vol. 5, nos 2–3, pp. 90–96, 2011.
[52] S. J. Byrnes, "Multilayer optical calculations," 2016, arXiv preprint, arXiv:1603.02720.
[53] S. Thongrattanasiri, F. H. L. Koppens, and F. J. García de Abajo, "Complete optical absorption in periodically patterned graphene," *Phys. Rev. Lett.*, vol. 108, 2012, Art no. 047401.
[54] I. Nechepurenko, D. Baranov, and A. Dorofeenko, "Lasing induced by resonant absorption," *Optic Express*, vol. 23, no. 16, pp. 20394–20401, 2015.
[55] Y. Chong, L. Ge, H. Cao, and A. D. Stone, "Coherent perfect absorbers: time-reversed lasers," *Phys. Rev. Lett.*, vol. 105, no. 5, 2010, Art no. 053901.
[56] W. Wan, Y. Chong, L. Ge, H. Noh, A. D. Stone, and H. Cao, "Time-reversed lasing and interferometric control of absorption," *Science*, vol. 331, no. 6019, pp. 889–892, 2011.
[57] B. Peng, Ş. Özdemir, S. Rotter, et al., "Loss-induced suppression and revival of lasing," *Science*, vol. 346, no. 6207, pp. 328–332, 2014.
[58] M. Brandstetter, M. Liertzer, C. Deutsch, et al., "Reversing the pump dependence of a laser at an exceptional point," *Nat. Commun.*, vol. 5, no. 1, pp. 1–7, 2014.
[59] A. Mostafazadeh, "Spectral singularities of complex scattering potentials and infinite reflection and transmission coefficients at real energies," *Phys. Rev. Lett.*, vol. 102, no. 22, p. 220402, 2009.
[60] S. Longhi, "Exceptional points and photonic catastrophe," *Optics Lett.*, vol. 43, no. 12, pp. 2929–2932, 2018.
[61] B. Zhen, C. W. Hsu, Y. Igarashi, et al., "Spawning rings of exceptional points out of Dirac cones," *Nature*, vol. 525, pp. 354–358, 2015.
[62] H. Zhou, C. Peng, Y. Yoon, et al., "Observation of bulk Fermi arc and polarization half charge from paired exceptional points," *Science*, vol. 359, pp. 1009–1012, 2018.
[63] H. O. Hågenvik and J. Skaar, "Fourier–Laplace analysis and instabilities of a gainy slab," *JOSA B*, vol. 32, no. 9, pp. 1947–1953, 2015.
[64] A. Maciejewski, R. Naskrecki, M. Lorenc, et al., "Transient absorption experimental set-up with femtosecond time resolution. Femto- and picosecond study of DCM molecule in cyclohexane and methanol solution," *J. Mol. Struct.*, vol. 555, pp. 1–13, 2000.
[65] V. I. Klimov, A. A. Mikhailovsky, S. Xu, et al., "Optical gain and stimulated emission in nanocrystal quantum dots," *Science*, vol. 290, no. 5490, pp. 314–317, 2000.
[66] A. Karim, S. Bjorlin, J. Piprek, and J. E. Bowers, "Long-wavelength vertical-cavity lasers and amplifiers," *IEEE J. Sel. Top. Quant. Electron.*, vol. 6, no. 6, pp. 1244–1253, 2000.
[67] H. Benisty, A. Degiron, A. Lupu, et al., "Implementation of PT symmetric devices using plasmonics: principle and applications," *Optic Express*, vol. 19, no. 19, pp. 18004–18019, 2011.
[68] Z. Ruan, "Spatial mode control of surface plasmon polariton excitation with gain medium: from spatial differentiator to integrator," *Optics Lett.*, vol. 40, no. 4, pp. 601–604, 2015.

Supplementary material: The online version of this article offers supplementary material (https://doi.org/10.1515/nanoph-2020-0253).